JOURNAL OF PROPULSION AND POWER
Vol. 25, No. 5, September–October 2009

Flame Spectra of a Turbulent Liquid-Fueled Swirl-Stabilized Lean-Direct Injection Combustor

Tongxun Yi* and Domenic A. Santavicca†
Pennsylvania State University, University Park, Pennsylvania 16802

DOI: 10.2514/1.43003

Flame spectra within the UV/visible-light range are measured for a turbulent, liquid-fueled, swirl-stabilized, lean-direct injection combustor. The flame spectra are quite similar to those of lean premixed combustion, which can be attributed to the small droplet size and fast fuel/air mixing. Broadband background emissions around 431 nm, which mainly consist of CO_2^* chemiluminescence, are found to be self-similar with wavelength for both stable and unstable combustion. Chemiluminescence from OH^*, CH^*, and CO_2^* is found to be a nonlinear function of the airflow rate, the equivalence ratio, preheat temperature, and pressure. Procedures for the determination of the instantaneous heat release rate and equivalence ratios along the flame front are developed. For both combustion instability and forced flame responses, the prediction errors are within 2.0% in the mean heat release rate, the mean air consumption rate, and the mean equivalence ratio. The assumption that chemiluminescence is proportional to the instantaneous heat releaser rate is generally invalid. Probably the proportionality is valid only in the weakly turbulent or wrinkled flamelet region in the absence of equivalence ratio variations and strong acoustic oscillations.

Nomenclature

$\mathrm{CH}(s)$	=	Laplace transform of CH^* chemiluminescence
$I(t)$	=	instantaneous chemiluminescence intensity, AU
L_f	=	curvilinear flame front
$\dot{m}_a(t)$	=	instantaneous air consumption rate, g/s
$\tilde{m}_a(t)$	=	instantaneous air consumption rate divided by 100 g/s
$\tilde{p}(t)$	=	instantaneous combustor pressure divided by the atmospheric pressure
$p'_a(t)$	=	acoustic pressure near the heat release zone, Pa
$p_f(t)$	=	instantaneous fuel pressure 0.29 m upstream of the fuel nozzle, Pa
$\dot{Q}_R(t)$	=	instantaneous heat release rate, kW
S_L	=	laminar burning velocity, m/s
s	=	symbol of the Laplace transform
$\bar{T}$	=	mean temperature in the heat release zone, K
$T'_a(t)$	=	acoustic temperature near the heat release zone, K
T_i	=	preheat temperature, K
$X(s)$	=	Laplace transform of $x(t)$
$\lvert W(s)\rvert$	=	gain of the transfer function $W(s)$
$\angle W(s)$	=	phase angle of the transfer function $W(s)$, deg
α	=	thermal diffusivity, m^2/s
ΔH_R	=	lower heating value of fuel, J/kg
δ_L	=	thickness of the laminar flame, m
ϕ	=	fuel/air equivalence ratio
$\tilde{\lambda}$	=	wave length divided by 431 nm
λ	=	wavelength, nm
ρ_a	=	air density, kg/m^3
ρ_u	=	reactant density, kg/m^3
τ_c	=	chemical reaction time, s

Received 2 January 2009; revision received 9 April 2009; accepted for publication 15 May 2009.

*Postdoctoral Fellow, Department of Mechanical and Nuclear Engineering; tzy1@psu.edu. Member AIAA.

†Professor, Department of Mechanical and Nuclear Engineering; das8@psu.edu. Member AIAA.

I. Introduction

THE instantaneous heat release rate and equivalence ratios are key parameters for combustion analysis and control. HCO is a good indicator of the instantaneous heat release rate, even in the presence of large strain rates [1]. However, both HCO^* chemiluminescence and planar laser-induced fluorescence (PLIF) suffer from low signal-to-noise ratios. An alternative method is to use the PLIF product of OH and CH_2O, as demonstrated by Paul and Najm [2] and Ayoola et al. [3]. However, this method requires a rather complicated optical setup including lasers, cameras, lenses, and optical filters. In contrast, chemiluminescence-based heat release measurements may just require an optical access, an optical fiber, an interference bandpass filter, and a detector such as a photomultiplier tube (PMT). Chemiluminescence is the spontaneous emission of photons from electronically excited species when they return to the background state. The formation of radial species, such as OH^*, CH^*, and C_2^*, are directly associated with chemical reactions.

The equivalence ratio can be determined from the PLIF signal, line-of-sight infrared absorption, and chemiluminescence from radial species. With excitations at 266 nm, the one- and two-ring aromatics in kerosene generate PLIF signals within 270–420 nm, which can be used to determine the droplet/vapor concentration [4]. The stretching C-H band, which is strongly absorbing around 3.39 μm, is prevalent in almost all hydrocarbon fuels. A path-integrated equivalence ratio can be determined from the line-of-sight extinction measurements [5]. The absorption method can also be extended to determine fuel vapor concentration for liquid/vapor mixtures [6]. Usually two laser beams, with one in the infrared light range and the other in the visible-light (VIS) range, are used. Chemiluminescence from radial species has been used to determine equivalence ratios for different combustion systems, including premixed laminar, premixed turbulent, and even spray flames [7–9]. Compared with PLIF and absorption measurements, chemiluminescence-based methods do not require a complicated optical setup. Local measurements of chemiluminescence can be performed using Cassegrain receiving optics, as demonstrated by Hardalupas and Orain [10]. Local measurements of chemiluminescence along the flame front can be used to examine the fuel/air mixing uniformity.

For unstretched, premixed, laminar flames, the flame zone structure, the flame speed, and the relationship between chemiluminescence and heat release are intrinsic properties of the fuel/air mixture. However, the situation is different for turbulent flames. In modern combustion theory, turbulent flames are conceived as a series of cascaded laminar flamelets, which drift with the local velocity and propagate normally toward the reactant. The location and orientation

of these laminar flamelets are solved using the level set method, that is, the G equation [11]. The local flame speed is determined from a "flamelet library" based on the local temperature, the local equivalence ratio, and the local stretch rate. In the wrinkled flamelet region, the flame is only slightly distorted by vortices or the velocity gradients; thus, the mass/heat diffusion and the flame zone structure can be assumed unaltered. In such a scenario, linearity between chemiluminescence and the heat release rate holds. In corrugated and broken flamelet regions, the flame zone structure, heat/mass diffusion across the flame front, and the flame speed are considerably affected by the local stretch rate and upstream flow inhomogeneities. In such cases, nonlinearity between chemiluminescence and heat release cannot be ignored. Samaniego et al. [12] reported that, for premixed flames, the unsteady effects of strain rates on CO_2^* chemiluminescence can be neglected. This is very different from diffusion flames, for which nonlinearity in flame response to upstream velocity perturbations prevails [13]. Several researchers have observed that the global chemiluminescence intensity is not sensitive to the strain rate. For example, Hardalupas and Orain [10] reported that, for premixed, laminar, counterflowing methane/air flames, the ratio of background-emission-corrected chemiluminescence, OH^*/CH^*, is not sensitive to the stretch rates within 80–400 s^{-1}. Lee et al. [14] reported that CH^* chemiluminescence per unit airflow rate is not sensitive to the airflow rate in a turbulent, premixed, dump combustor fueled with methane. Probably in their turbulent combustor, although very large strain rates associated with vortex motions and large velocity gradients due to flow inhomogeneities do exist, the major portion of the flame still lies within the wrinkled flamelet region.

Measurements of chemiluminescence from OH^*, CH^*, and C_2^* are common in combustion experiments, in particular in combustion instability research. Combustion instability refers to the self-excited, positively coupled, large-amplitude, limit-cycle oscillations of combustor pressure and heat release. The instantaneous heat release rate is a key parameter, determining both the onset and the limiting amplitude of combustion instability. It is typically assumed that chemiluminescence is proportional to the instantaneous heat release rate. This assumption, in fact, suffers from several major deficiencies.

First, the relationship between chemiluminescence and the heat release rate is not necessarily linear, because chemical reactions usually follow different paths. Also, the elementary reactions for the production and removal of radical species may involve more than one radical atom.

Second, even if the relationship between chemiluminescence and heat release is linear, the proportionality depends on the physicochemical conditions, such as the flame temperature and pressure. At lower pressures, the chance of collisions between a radical atom and other species is reduced; thus, a radical atom has a larger opportunity to release the photon than at higher pressures. For laminar, premixed methane/air flames, a power index of -0.86 and -0.64 of pressure is reported for OH^* and CH^* chemiluminescence, respectively [15,16]. The chemiluminescence yield is proportional to a positive power of the flame temperature or the equivalence ratio. For steady combustion, the flame temperature is uniquely determined by the equivalence ratio and the preheat temperature. Here we do not consider the endothermic dissociation reactions. For premixed ethane/CO/air combustion, chemiluminescence from C_2^* and CH^* is found to be a fourth power of the ethane concentration [17]. For laminar, premixed methane/air flames, a power index of 5.23 and 2.72 of the equivalence ratio is reported for OH^* and CH^* chemiluminescence, respectively [15,16].

Third, acoustic oscillations are isentropic, but both the acoustic pressure and temperature affect the chemiluminescence yield. Thus, acoustics-induced chemiluminescence oscillations should be discounted for the quantitative determination of the heat release rate.

Fourth, chemiluminescence measurements using interference filters, say around 306 nm for OH^* chemiluminescence and around 431 nm for CH^* chemiluminescence, are inevitably contaminated by broadband background emissions. The background emissions include chemiluminescence from CO_2^* and HCO^* and probably a small amount of gray-body radiation from soot and hot surfaces. For turbulent, swirl-stabilized, lean-direct fuel injection (LDI) combustion, the fuel-rich pockets are significantly reduced because of the low equivalence ratio and highly efficient fuel/air mixing.

The present paper is organized as follows. First, a liquid-fueled, swirl-stabilized, LDI combustion rig and the optical setup are described; second, flame spectra for both stable and unstable combustion are presented and analyzed; third, PMT-based chemiluminescence measurements are presented and analyzed; and fourth, methods for the quantitative determination of the instantaneous heat release rate and equivalence ratios along the flame front are developed that account for acoustics-induced chemiluminescence oscillations and the nonlinearity among chemiluminescence, the equivalence ratio, and the heat release rate.

II. Experiment Setup

Figure 1 shows the liquid-fueled, swirl-stabilized, LDI combustion rig and the optical setup. Preheated air enters a quartz combustion chamber that is 0.10 m in diameter and 0.30 m in length through a 30 deg tangential-entry swirler. The exit diameter of the swirler is 3.56 cm. The pressure drop across the air swirler varies with the airflow rate and the preheat temperature, but it is within 5% for all results reported here. Jet A is injected into swirling airflow 0.02 m upstream of the dump plane using a 2.5 gal/h single-point macrolaminated fuel nozzle from Parker Hannifin Corporation. With a pressure drop of 689 kPa across the fuel nozzle, the droplet Saunter mean diameter is less than 10 μm for water.[‡] The airflow rate is measured using a Vortex flowmeter from Omega, with a measurement uncertainty of 1.0 scfm. The preheat temperature is measured using a type-K thermocouple 7.6 cm upstream of the dump plane and is regulated using a proportional-integral-derivative controller. Stable combustion is achieved by inserting three baffle plates downstream of the quartz tube. Without explicit denotations, all data reported are obtained from stable combustion.

Global emissions are sampled using a UV/VIS optical fiber with a viewing angle of 25 deg (and a numerical aperture of 0.22). The optical fiber is oriented perpendicular to and 0.41 m away from the quartz tube. The beam-forming devices include three spherical lenses. The beam is converged to a waist diameter of less than 1 mm and enters an Oriel MS125™ spectrograph through a 100-μm-wide slit. The spectrometer is featured with a ruled grating (model no. 77416) with 400 lines/mm and a 350 nm blaze. This spectrometer is suitable for spectral measurements within 200–800 nm. An intensified charge-coupled device (ICCD) camera with 576×384 pixels from Princeton Instruments is used for spectral imaging. An Oriel Hg(Ar) lamp (model no. 6035) is used for spectral line calibration. At the exit of the spectrometer, light from the Hg(Ar) lamp is decomposed into a number of bright narrow bands at 435.84, 404.66, 365.02, 313, and 284.8 nm, respectively. A linear curve-fitting polynomial expressing wavelength as a function of the horizontal pixel index of an ICCD image is determined as $\lambda(\text{nm}) = 261.41 + 0.38507x$. Here, x refers to the horizontal pixel index in an ICCD image. Detector noises due to dark current are accounted for by subtracting the background image, which is taken without exposure to light but at the same exposure duration and the intensifier gain. Chemiluminescence from OH^*, CH^*, and CO_2^* is also measured using a PMT housing. The PMT housing is placed about 2.3 m away and perpendicular to the quartz tube. Light emissions from the quartz tube are split into three streams using two UV plate beam splitters. Each light stream is focused using spherical lenses onto a 2×6 mm^2 rectangular image, which lies exactly in the central region of the PMT effective area. This enables global chemiluminescence measurements and linear responses between light intensity and the output voltage. Optimal focusing is achieved by adjusting the location of the PMT housing until the smallest and brightest image is obtained. Three bandpass filters with a full width half minimum of 10 nm are placed in front of the PMTs. The center wavelength is around 307 nm for OH^*, around 365 nm for CO_2^*, and around 431 nm for CH^*. Light absorption across air is negligibly small within the

[‡]Engineers from Parker Hannifin Corporation, private communication, 12 April 2008.

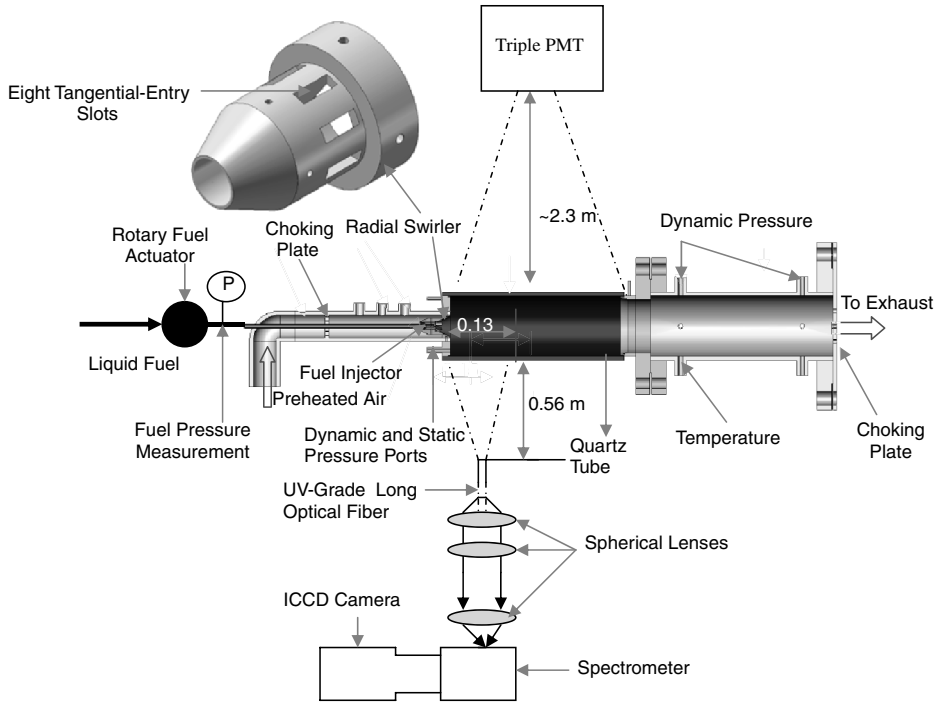

Fig. 1 The combustion rig and the optical setup.

UV/VIS range. Combustion experiments are performed in a dark room.

III. Flame Spectra

A. Broadband Background Emissions

Figure 2 shows the flame spectra for stable combustion fueled with Jet-A. The narrow-band peaks around 306, 431, and 474 nm are associated with chemiluminescence from OH* ($A^2\Sigma^+ - X^2\Pi$), CH* ($A^2\Delta - X^2\Pi$), and C_2^*, respectively. Each narrow-band peak extends over a finite wavelength range, which can be attributed to thermally excited rovibrational band broadening, natural broadening due to energy-time uncertainty, thermal Doppler broadening due to atomic velocities, and pressure broadening. The flame spectra are quite similar to those of lean premixed combustion. The smaller peak around 306 nm does not necessarily imply that OH* chemiluminescence is weaker than CH* chemiluminescence. This is associated with the transmission efficiency of the optical system and the quantum efficiency of detectors. The overall efficiency of an optical measurement system is a function of wavelength, which can be determined using a blackbody or a calibrated tungsten lamp.

Also shown in Fig. 2 is an ICCD image of OH* chemiluminescence. Here $\phi = 0.33$ and the preheat temperature is 423 K. The axial center of heat release lies 2.5 cm downstream of the dump plane. If the average axial velocity along the swirling shear layer is taken as 40% of the swirler exit velocity, that is, 21 m/s, then the convective time delay is about 1 ms. If we assume a representative droplet size of 18 μm and a representative temperature of 900 K, the evaporation time is determined as 1.0 ms and the evaporation constant is determined as $3.2092e-7$ m^2/s by following the procedures in [18]. This computation neglects droplet velocity slip, droplet interactions, droplet/vortex interactions, initial transients, and radiative heat transfer. The boiling point of Jet-A is taken as 503 K, density as 800 kg/m^3, thermal conductivity of fuel vapor as 0.063 W/m $\cdot$ K, the constant-pressure specific heat as 3138.3 J/kg $\cdot$ K, and the latent heat of vaporization as 260 kJ/kg. From the time scale analysis, one can see that, before the droplets are transported to the major heat release zone, the evaporation process has completed. If we assume a laminar flame speed of 0.5 m/s, then the time scale of chemical kinetics is estimated as $\tau_c = \frac{\delta_L}{S_L} \approx \frac{2\alpha(@900\ \mathrm{K})}{S_L^2} = 1.14$ ms. The time scales of evaporation and chemical kinetics increase with decreases in the flame temperature. Fuel/air mixing is very efficient in the present combustor. Figure 1 shows that air enters the swirler through eight tangential-entry slots, mixes with the fine sprays, recombines into one stream, and then suddenly expands at the dump plane. A significant amount of streamwise vorticity is generated when air enters the swirler through eight tangential-entry ports. Droplets/vapor/air entrainment and

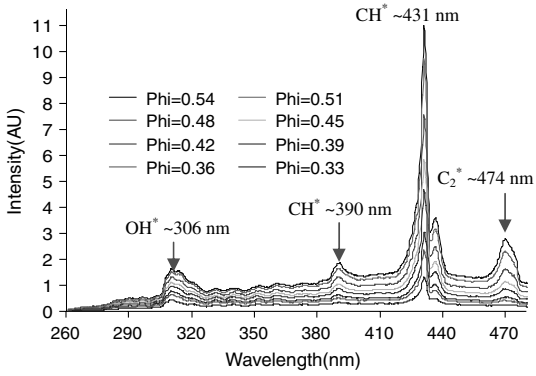

a)

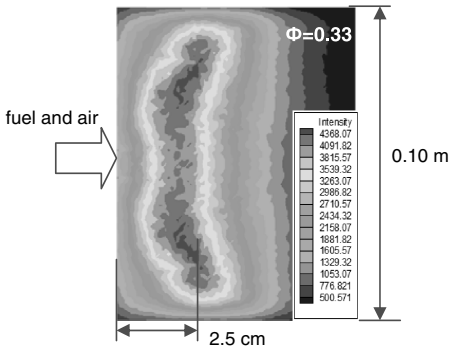

b)

Fig. 2 Flame spectrum and ICCD image of OH* chemiluminescence for Jet-A-fueled LDI combustion: a) flame spectra, and b) ICCD imaging. The airflow rate is 44.5 g/s, and the preheat temperature is 423 K.

mixing are also very efficient along the swirling shear layer. This results in a rather homogeneous fuel/air mixture upstream of the flame front. This explains why the flame spectra shown in Fig. 2 are very similar to those of lean premixed gaseous combustion.

The broadband spectra extending from 280 to 490 nm mainly consist of CO_2^* chemiluminescence, HCO^* chemiluminescence, and possibly a very small amount of gray-body radiation from soot and hot surfaces. Some small peaks between 320 and 410 nm are associated with HCO^* chemiluminescence. Chemiluminescence from CO_2^* and HCO^* can be used as heat release rate indicators. In this sense, the term "background emissions" may be a misnomer. Background emissions around 307 nm (within a wavelength range of 16 nm) are approximated using a linear curve-fitting polynomial based on the UV spectra within 281–295 and 338–377 nm. Background emissions around 431 nm (within a wavelength range of 15 nm) are approximated using a quadratic curve-fitting polynomial based on the VIS spectra within 396–419 and 442–462 nm. Figure 3 shows the ratio of background emissions to the gross intensity within 300–316 and 422–438 nm, respectively. Experiments are repeated multiple times within 1 month, with the airflow rate at 27.8, 33.4, 38.9, 44.5, and 55.6 g/s and the preheat temperature at 373, 381, 398, 423, 448, and 473 K. At the same equivalence ratio, the ratio of background emissions varies with the airflow rate and the preheat temperature. The variations are within 5% around 307 nm and within 10% around 431 nm. The difference in the background ratio around 431 nm increases with decreasing equivalence ratios, but that around 307 nm does not. With decreasing equivalence ratios from 0.54 to 0.33, the background ratio around 431 nm increases more than 30%, whereas that around 307 nm increases less than 4%. This is because CH^* chemiluminescence is more affected by the hydrocarbon concentration than OH^* chemiluminescence. In other words, CH^* chemiluminescence is a higher-order nonlinear function of the equivalence ratio than OH^* chemiluminescence. This can be seen from the correlation functions to be presented in Eqs. (2–4) in Sec. IV.

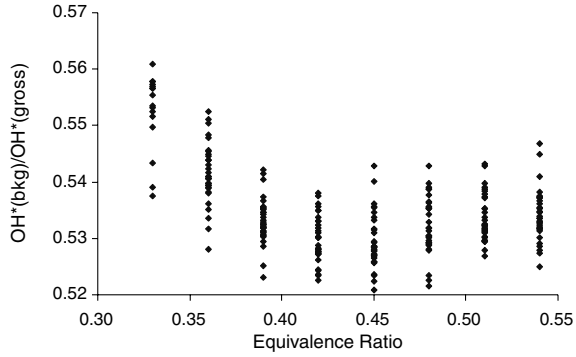

a)

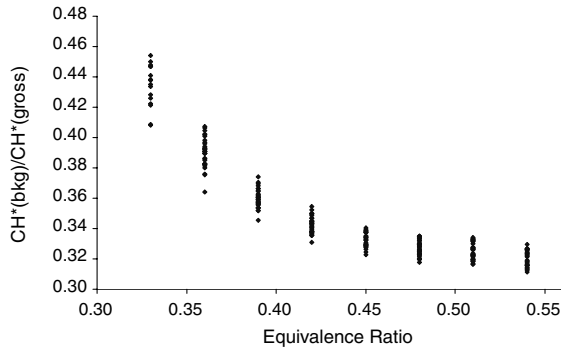

b)

Fig. 3 Ratio of background emissions at the approach of LBO: a) around 306 nm, and b) around 431 nm. There are large variations in the equivalence ratio, the airflow rate, and the preheat temperature among the experiments.

B. Self-Similarity of Broadband Spectra Around 431 nm

The broadband spectra around 431 nm (within a wavelength range of 15 nm) are approximated using a second-order curve-fitting polynomial:

$$I(\bar{\lambda}) = a_0 + a_1\bar{\lambda} + a_2\bar{\lambda}^2 \tag{1}$$

Here $\bar{\lambda} = \lambda/431$. λ refers to the wavelength in nanometers. The polynomial coefficients vary with the airflow rate, the preheat temperature, the equivalence ratio, and pressure. This model is of second order in wavelength; thus, it is applicable only within a short wavelength range. Table 1 shows the normalized polynomial coefficients with decreasing equivalence ratios from 0.51 to 0.33. The curve-fitting coefficients are normalized by those at $\phi = 0.39$. For the first experiment, the airflow rate is 55.6 g/s and the preheat temperature is 473 K. For the second experiment, the airflow rate is 27.8 g/s and the preheat temperature is 398 K. Table 1 shows that, at the same airflow rate and the preheat temperature, the three normalized coefficients vary with the equivalence ratio at almost the same rate, with differences of less than 3.0%. The ratio of the baseline polynomial coefficients for the two experiments is also almost the same, that is, [1.3239 1.3247 1.3211]. The differences are less than 0.3%. The self-similarity in the distribution of chemiluminescence intensity with wavelength implies that, if the broadband emissions near 431 nm, say, within 396–406 or 450–460 nm, are measured using a PMT, then background emissions around 431 nm can be accurately determined. We also notice that self-similarity does not exist around 307 or around 365 nm.

C. Flame Spectra During Combustion Instability

Figure 4 shows phase-locked flame spectra during self-excited combustion instability at 10, 100, and 190 deg of the acoustic pressure measured at the dump plane. The unstable frequency is 550 Hz, corresponding to the half-wave mode of the combustion chamber (0.56 m long). The airflow rate is 44.5 g/s, the equivalence ratio is 0.35, and the preheat temperature is 398 K. The three flame spectra correspond to the maximum, medium, and minimum heat release within a pressure cycle, respectively. The second-order curve-fitting polynomial coefficients for the three phase-locked flame spectra around 431 nm are determined as [−1.8047e + 001 3.3991e + 001 −8.6690e + 000], [−1.3353e + 001 2.4492e + 001 −6.3188e + 000], and [9.7051e + 000 1.7969e + 001 −4.5892e + 000], respectively. Again the distribution of the broadband background emissions around 431 nm is self-similar with wavelength.

IV. Photomultiplier-Tube-Based Chemiluminescence Measurements

Correlation functions, which express the chemiluminescence intensity as a function of the airflow rate, the equivalence ratio, the preheat temperature, acoustic pressure, and acoustic temperature, are developed from PMT-based chemiluminescence measurements. The

Table 1 Normalized curve-fitting coefficients for background emissions around 431 nm

ϕ	Air 27.8 g and 398 K			Air 55.6 g/s and 473 K		
	$\bar{a}_0$	$\bar{a}_1$	$\bar{a}_2$	$\bar{a}_0$	$\bar{a}_1$	$\bar{a}_2$
0.51	2.3263	2.3580	2.3692	2.1259	2.1588	2.1755
0.48	1.7885	1.8164	1.8208	1.8014	1.8304	1.8581
0.45	1.6792	1.6904	1.7097	1.5516	1.5709	1.5908
0.42	1.3932	1.4064	1.4276	1.2988	1.3065	1.3185
0.39	1.0000	1.0000	1.0000	1.0000	1.0000	1.0000
0.36	0.7716	0.7697	0.7676	0.7519	0.7455	0.7423
0.33	0.5846	0.5823	0.5785	0.6040	0.5990	0.5926
	a_0	a_1	a_2	a_0	a_1	a_2
0.39	−116.23	233.73	−107.97	−153.88	296.37	−134.71

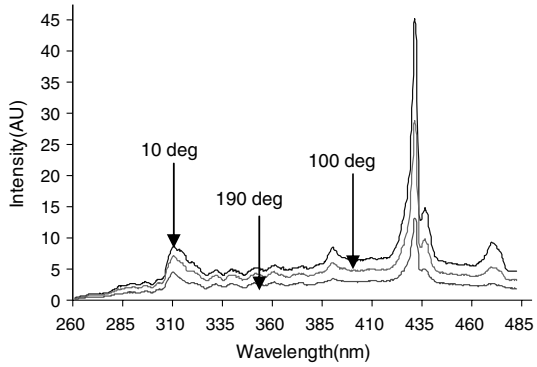

Fig. 4 Flame spectra at three phases from pressure at the dump plane, that is, at 10, 100, and 190 deg, respectively. The ICCD exposure time duration is 200 μs, the intensifier gain is 9, and the accumulation is 500.

correlation functions are based on several assumptions, including complete combustion, a fixed percentage of heat loss, and a fixed constant-pressure specific heat. Complete combustion implies that the global heat release rate is proportional to the fuel flow rate. The assumptions of a fixed percentage of heat loss and a fixed constant-pressure specific heat imply that the rise in the flame temperature is proportional to the equivalence ratio. For the present liquid-fueled LDI combustor, because of the small droplet size and highly efficient fuel/air mixing, the fuel/air equivalence ratio is almost uniform upstream of the flame front. Thus, a globally representative equivalence ratio can be assumed. To incorporate pressure effects into the correlation functions, a perforated plate with different blocking ratios is installed at the combustor exit. The combustor pressure can vary up to 40% of the atmospheric pressure. The combustor static pressure is measured using a Sensotec pressure transducer (with a sensitivity of 172 kPa/V and an uncertainty of 0.5 kPa), which is installed 1.5 m away from the combustion chamber using an extension tube. The dynamic pressure near the heat release zone is measured using a high-sensitivity PCB pressure sensor (112A05/422E51). Chemiluminescence from OH^*, CH^*, and CO_2^* is measured within a broad range of working conditions, with the airflow rate from 27.8 to 66.7 g/s, the equivalence ratio from 0.32 to 0.50, and the preheat temperature from 373 to 473 K. Experiments are repeated eight times within 1 month, and 1100 data sets are obtained. Because background emissions mainly consist of CO_2^* chemiluminescence, which itself can be used as an indicator of the heat release rate, no corrections to background emissions are made. Correlation functions are developed as follows:

$$I_{307\,\mathrm{nm}} = 94.61\tilde{\dot{m}}_a^{1.7558}\phi^{2.1369}(\phi + (T_i/2000))^{1.1060}\tilde{p}^{-0.4522} \quad (2)$$

$$I_{365\,\mathrm{nm}} = 115.85\tilde{\dot{m}}_a^{1.3637}\phi^{2.2280}(\phi + (T_i/2000))^{0.8217}\tilde{p}^{-0.2183} \quad (3)$$

$$I_{430\,\mathrm{nm}} = 212.05\tilde{\dot{m}}_a^{1.6627}\phi^{3.0735}(\phi + (T_i/2000))^{1.4352}\tilde{p}^{-0.4045} \quad (4)$$

where $\tilde{\dot{m}}_a$ refers to the normalized airflow rate, that is, the airflow rate divided by 100 g/s. $\tilde{p}$ refers to the normalized pressure, that is, the combustor pressure divided by one atmospheric pressure. For unsteady combustion, that is, self-excited combustion instability and forced flame responses under fuel modulations, $\dot{m}_a(t)$ should be interpreted as the instantaneous air consumption rate along the flame front, that is,

$$\dot{m}_a = \int_0^{L_f} \rho_a(l)s_L(l)\delta(l)\,\mathrm{d}l \quad (5)$$

where S_L and ρ_a refer to the laminar flame speed and the air density along the flame front, respectively. $\delta(l)$ denotes the depth of the flame sheet. Note that the instantaneous air consumption rate along the flame front may differ considerably in both amplitude and phases from the instantaneous airflow rate at the combustor inlet. For Jet-A combustion, the air density ρ_a differs from the reactant density ρ_u by 2–3%, with the equivalence ratio ranging from 0.30 to 0.50. Based on the assumptions of a fixed percentage of heat loss and a fixed constant-pressure specific heat, $(\phi + (T_i/2000))$ is proportional to the flame temperature. Here we assume an increase of 2000 K in the adiabatic flame temperature for stoichiometric fuel/air mixtures. Equations (2–4) show that the chemiluminescence intensity is a nonlinear function of the airflow rate, the equivalence ratio, the flame temperature, and pressure. In particular, chemiluminescence is most sensitive to equivalence ratio variations.

Figure 5 compares the measured chemiluminescence versus the curve-fitting results. As described earlier, we have performed 1100 experiments. The average error (for the whole data set) between measurements and curve fitting is within 2.37% for OH^*, within 1.96% for $CO2^*$, and within 3.8% for CH^*. The relatively large error in CH^* correlation can be attributed to the different emission characteristics between $CO2^*$ and CH^* chemiluminescence. However, an error of 3.8% should be acceptable for many applications. The fact that accurate curve-fitting models are obtainable within a large range of working conditions can be attributed to the fast evaporation process, efficient fuel/air mixing, and small variations in the flame structure [19]. Here the flame structure refers to the spatial distribution of the heat release zone. It is found that, even during self-excited combustion instability, variations in the flame structure mainly occur in the chemiluminescence intensity rather than in the spatial distribution of the heat release zone.

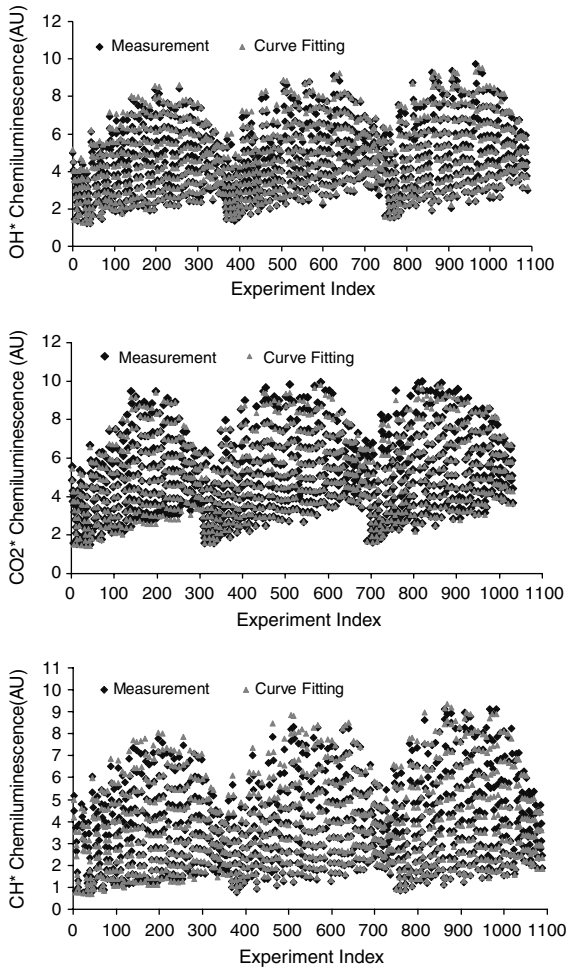

Fig. 5 Chemiluminescence measurements vs curve fitting. Data are obtained within a large range of airflow rates, equivalence ratios, preheat temperature, and pressure. More than 30% of the data are obtained from unstable combustion. The experiment index simply refers to the sequence in which each experiment is performed.

V. Determination of the Instantaneous Heat Release Rate and Equivalence Ratios

The instantaneous heat release rate and equivalence ratios are key parameters for combustion analysis and control. For self-excited combustion instability, equivalence ratio variations are caused by the differential acoustic impedance between the fuel and air lines. The unsteady heat release can be caused by multiple mechanisms, including variations in the flame surface area, the reaction heat, and the laminar burning speed. Whether the correlation functions can be applied to unsteady combustion requires further exploration. In the present combustor, evaporation is no longer the limiting process, and fuel/air mixing is efficient. At the same working conditions, the differences in the mean chemiluminescence intensity between steady and unsteady combustion are usually within 2.0%. Large vortex shedding synchronized with pressure cycles has been identified as a dominant mechanism for combustion instability in bluff-body-stabilized and dump combustors [20]. However, for swirl-stabilized combustors, the shear-layer growth and decay rates are significantly enhanced [21,22]. There are fewer opportunities for the Kelvin–Helmholtz shear-layer mode to continuously grow and for the wakelike absolutely unstable mode to form. Several researchers have observed almost no variations in the flame structure in swirling combustion during both self-excited combustion instability and forced flame responses with air modulations [23,24]. Even for sharp-edged nonswirling combustors, large vortex shedding does not occur unless air forcing is applied around the preferential frequencies of the shear-layer dynamics and the forcing amplitude exceeds certain thresholds [25]. Even in the presence of large-scale vortex shedding, a major portion of the flame rides over the large vortices and the flame curvature radius is typically much larger than the flame thickness. Thus, the correlation functions developed from steady combustion can be applied to unsteady combustion, in particular for lean premixed combustion.

The instantaneous air consumption rate, the instantaneous equivalence ratio, and the instantaneous heat release rate are determined as follows:

$$
\begin{aligned}
\tilde{\dot{m}}(t) &= 0.1571(I_{307\,\mathrm{nm}}(t))^{1.4747}(I_{365\,\mathrm{nm}}(t))^{0.7294}(I_{430\,\mathrm{nm}}(t))^{-1.5540}(\tilde{p}(t))^{0.1974} \\
\phi(t) &= 0.1392(I_{307\,\mathrm{nm}}(t))^{-1.2966}(I_{365\,\mathrm{nm}}(t))^{1.4942}(I_{430\,\mathrm{nm}}(t))^{0.1437}(\tilde{p}(t))^{-0.2021} \\
\dot{Q}_R(t) &= 0.1\Delta H_R\tilde{\dot{m}}(t)\phi(t)\left(\frac{\bar{\dot{m}}_f}{\bar{\dot{m}}_a}\right)_{\mathrm{stoichiometry}} = 0.00674\Delta H_R\tilde{\dot{m}}(t)\phi(t) = 281.7\tilde{\dot{m}}(t)\phi(t)\ \mathrm{(kW)}
\end{aligned}
\tag{6}
$$

Equation (6) is obtained from Eqs. (2–4) by eliminating $(\phi + (T_i/2000))$. In our experiments, both the preheat temperature and pressure near the heat release zone are measured. In the case of self-excited combustion instability, the normalized flame temperature should be formulated as $(\phi + \frac{T_i+T'_a}{2000})$. Here $T'_a(t) = \bar{T}(1 + \frac{\gamma-1}{\gamma}\frac{p'_a}{\bar{p}})$ and $\gamma = 1.33$. $p'_a(t)$ is the acoustic pressure near the heat release zone. The lower heating value of Jet-A is taken as 41.8 MJ/kg. The chemical formula of Jet-A is assumed as $C_{11}H_{23}$; thus, the stoichiometric fuel/air ratio is 0.0674. The mean heat release rate is determined as

$$
\begin{aligned}
\bar{\dot{Q}}_R &= \Delta H_R\bar{\dot{m}}\,\bar{\phi}(\bar{\dot{m}}_f/\bar{\dot{m}}_a)_{\mathrm{stoichiometry}} \\
&= 0.0674\Delta H_R\bar{\dot{m}}\,\bar{\phi} = 2.8173\bar{\dot{m}}\,\bar{\phi}\ \mathrm{(kW)}
\end{aligned}
\tag{7}
$$

Here $\bar{\dot{m}}$ and $\bar{\phi}$ refer to the mean air consumption rate and the mean equivalence ratio, respectively.

A. Parameter Estimation for Self-Excited Combustion Instability

Figure 6 shows the estimated mean heat release rate and mean equivalence ratios with decreasing equivalence ratios from 0.41 to 0.31. Here the airflow rate is 66.7 g/s, and the preheat temperature is 373 K. The half-wave mode of the combustion chamber is excited when the equivalence ratio is decreased below 0.34. The estimation error is within 1.4% for the mean equivalence ratio, within 1.9% for the mean air consumption rate, and within 1.0% for the mean heat release rate.

Figure 7a shows the time traces of chemiluminescence and acoustic pressure near the dump plane at $\phi = 0.33$. The phase difference between CH^* chemiluminescence and pressure is 33.7 deg. The in-phase oscillations of acoustic pressure and heat release provide energy to maintain acoustic oscillations. Figure 7b shows the estimated instantaneous air consumption rate, the estimated instantaneous equivalence ratio, and the estimated instantaneous heat release rate. All these parameters are in phase. The oscillating amplitude of the air consumption rate is 35% of the mean, and that of the equivalence ratio is 17%.

Self-excited combustion instability grows stronger with decreasing equivalence ratios from 0.34 to 0.33. In Table 2, the equivalence ratio is expressed as a three-digit number. This does not necessarily imply that the measurement accuracy in equivalence ratios can be as high as 0.001. This is simply to denote the discernible differences in equivalence ratio measurements. With decreasing equivalence ratios from 0.34 to 0.33, the phase lag between the heat release rate and CH^* chemiluminescence increases from 10.2 to 0.74 deg, whereas the gain increases by more than 20%. This example shows that, during self-excited combustion instability, chemiluminescence is not proportional to the instantaneous heat release rate. The same conclusion can be drawn for forced flame responses with fuel modulations, which will be shown in Sec. V.B.

B. Parameter Estimation for Forced Flame Responses with Fuel Modulations

Fuel modulations are achieved using a motor-driven, high-frequency, rotary fuel valve specially designed for this experiment. A detailed description of the rotary valve and the fuel setup is included in [26]. The rotary valve (Fig. 8) is located 0.46 m upstream of the fuel nozzle. A 0.8 l accumulator is located 0.2 m upstream of the rotary valve. A Sensotec pressure transducer (with a sensitivity of 172 kPa/V and an uncertainty of 0.5 kPa) capable of working up to 2 kHz is installed 0.29 m upstream of the fuel nozzle. A bypass flow passage is installed parallel to the rotary fuel valve. The fuel modulation amplitude is controlled by varying the fuel split between the rotary valve and the bypass passage. The fuel modulation frequency is determined by the number of rotor teeth and the motor rotating speed. The valve is featured with 16 equally spaced teeth, capable of fuel modulations of up to 1 kHz. In this experiment, the combustion chamber is 1.05 m long.

Figure 9a shows the estimated mean parameters with fuel modulations up to 1 kHz. The exact air consumption rate is 44.5 g/s, the exact mean equivalence ratio is 0.40, and the exact mean heat release rate is 50.1 kW. The errors in the three estimated mean parameters are within 2.0%. Figure 9b shows the fuel modulation ratio, which is defined as the fuel pressure rms to the mean fuel

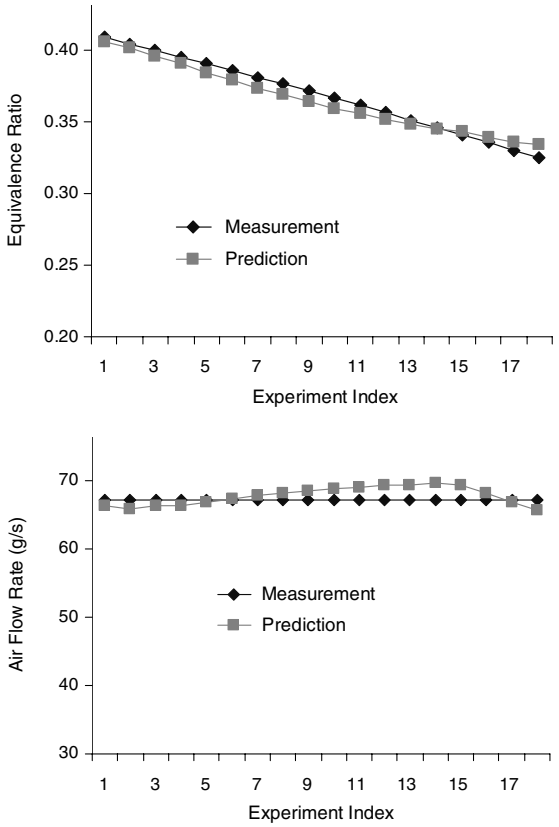

Fig. 6 The estimated mean air consumption rate and the mean equivalence ratio. The airflow rate is 66.7 g/s, the preheat temperature is 373 K, and the equivalence ratio is decreased from 0.41 to 0.31.

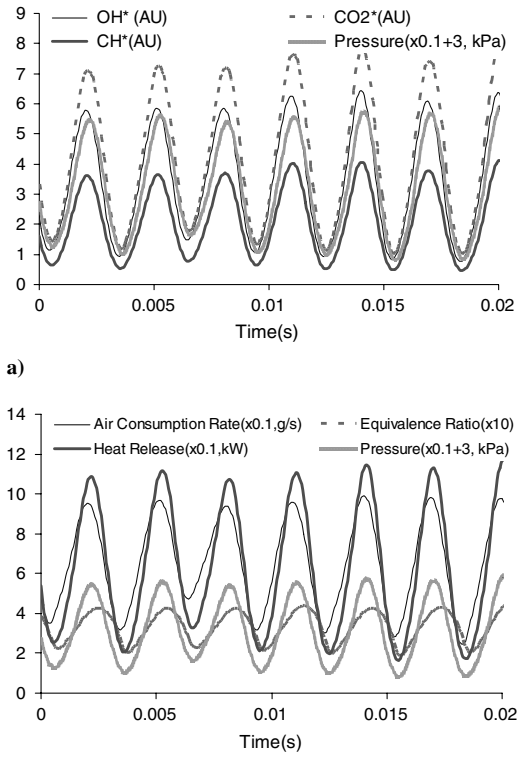

Fig. 7 Shown are the following: a) time traces of chemiluminescence and combustor pressure, and b) estimated instantaneous air consumption rate, the estimated instantaneous equivalence ratio, and the estimated instantaneous heat release rate.

Table 2 Estimated parameters for self-excited combustion instability

ϕ	P_{rms}, kPa	$\angle \text{CH}^*/\tilde{p}$	$\angle \dot{Q}_R/\tilde{p}$	$\angle \dot{Q}_R/\text{CH}^*$	$\lvert\dot{Q}_R/\text{CH}^*\rvert$
0.341	4.4751	50.5380	40.2940	−10.2440	22.7920
0.336	8.5880	41.4840	36.0660	−5.4176	23.6650
0.330	9.9346	33.6610	32.9170	−0.7439	27.1310

pressure. The fuel modulation amplitude affects both the gain and phases of the transfer function. Figure 10 shows the flame transfer functions, which are defined in multiple forms. In Figs. 10a–10c, the gain of the transfer functions consistently increases up to 700 Hz and then declines. Note that the fuel pressure 0.29 m upstream of the fuel nozzle differs in both gain and phases from that immediately upstream of the fuel nozzle, in particular at a high frequency [26]. "Abnormalities" or "irregularities" in the flame transfer functions, say, between 300 and 400 and between 620 and 700 Hz, can be attributed to the relatively strong forcing-induced acoustic oscillations. The flame transfer functions within these two frequency ranges are no longer open loop. Acoustic damping of this rig has been significantly enhanced by inserting three baffle plates downstream of

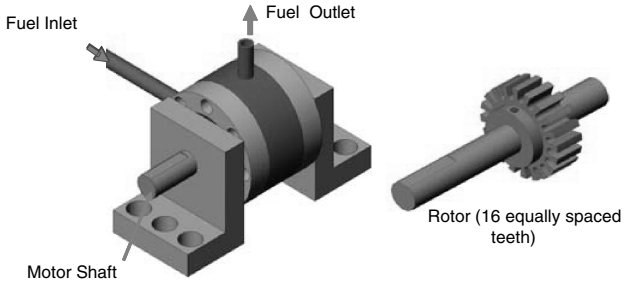

Fig. 8 Rotary fuel valve.

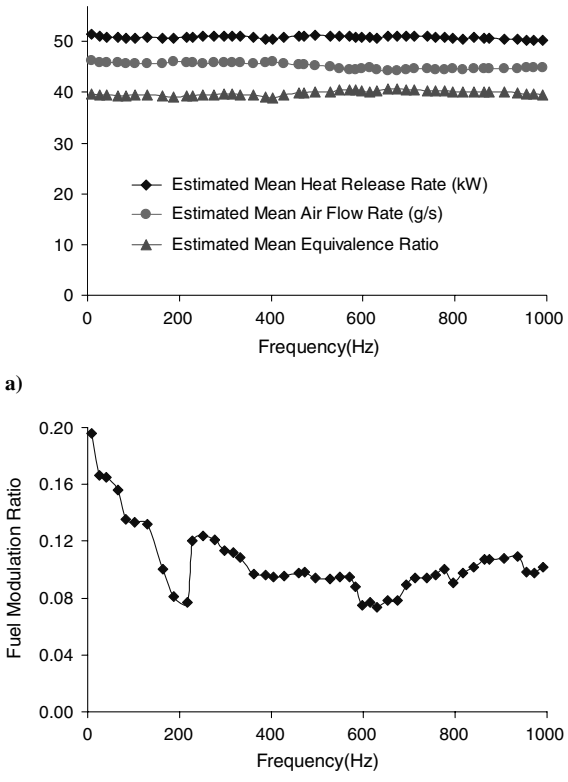

Fig. 9 Shown are the following: a) estimated mean equivalence ratio (multiplied by 100), the estimated mean air consumption rate, and the estimated mean heat release rate; and b) fuel modulation ratio for this experiment. At most frequencies, the fuel modulation ratio is above 10%.

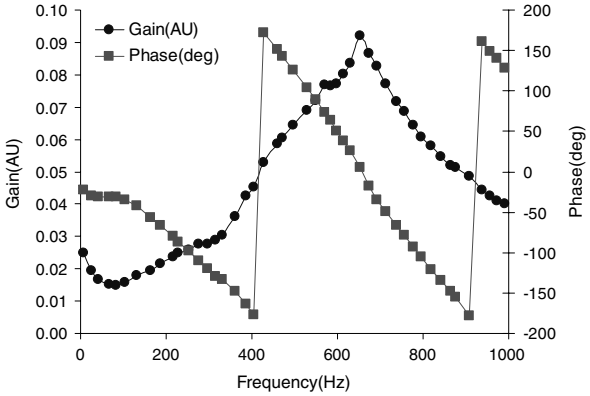

a) $CH^*(s)/P_f(s)$

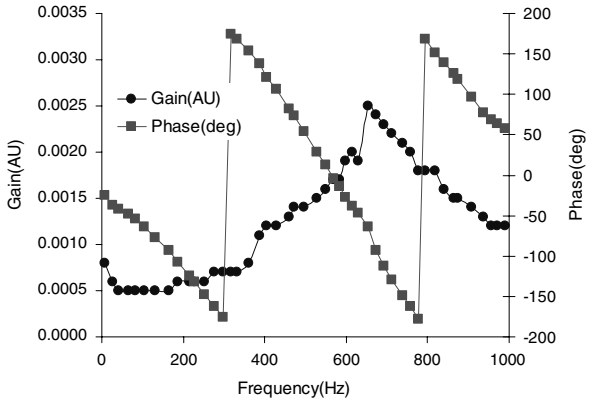

b) $\phi(s)/P_f(s)$

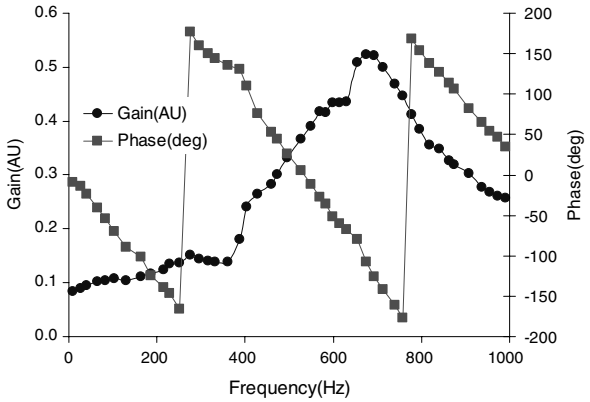

c) $\dot{Q}_R(s)/P_f(s)$

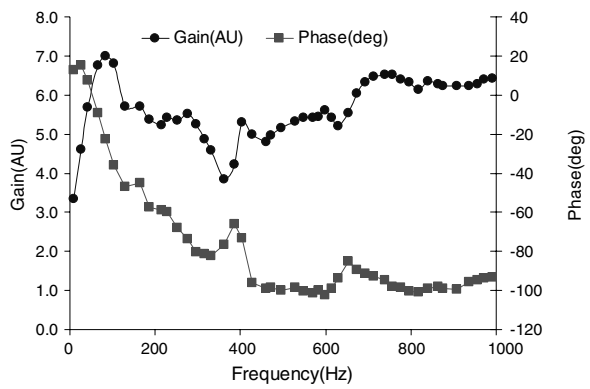

d) $\dot{Q}_R(s)/CH^*(s)$

Fig. 10 Flame transfer functions: a) CH* chemiluminescence (AU) to the fuel pressure (kPa), b) estimated equivalence ratio to the fuel pressure (kPa), c) estimated heat release rate (kW) to the fuel pressure (kPa), and d) estimated heat release rate (kW) to CH* chemiluminescence (AU).

the heat release zone. However, fuel modulations around the acoustic resonant frequencies, that is, around 330 (half-wave mode) and around 660 Hz (one-wave mode), still generate pressure oscillations up to several hundred Pa. As pointed out before, acoustic oscillations not only directly affect the chemiluminescence yield, but also modify the flame kinetics. In Figs. 10a–10c, the phases of the transfer function decrease with the frequency but at different rates.

The most interesting, yet somewhat puzzling, observation is the transfer function $\dot{Q}_R(s)/\mathrm{CH}^*(s)$. Figure 10d shows that, except around the acoustic resonant frequencies, the phase consistently decreases with the frequency and saturates at -96 deg above 400 Hz. Above 100 Hz, the gain variations are more than 20%. Recall that, for self-excited combustion instability (Table 2), both the gain and phases of $\dot{Q}_R(s)/\mathrm{CH}^*(s)$ vary with the acoustic oscillation intensity. Thus, the assumption of proportionality between chemiluminescence and the heat release rate is generally invalid. Probably the proportionality is valid only for weakly turbulent or wrinkled flamelet regions in the absence of equivalence ratio variations along the flame front and strong acoustic oscillations. Take steady combustion as an example. In one experiment with an airflow rate at 27.8 g/s and an equivalence ratio of 0.44, the mean CH* chemiluminescence is 3.23 AU and the mean heat release rate is 34.5 kW. In another experiment with an airflow rate at 44.8 g/s and an equivalence ratio of 0.38, the mean CH* chemiluminescence is 2.33 AU and the mean heat release rate is 48.0 kW. In other words, whereas the CH* chemiluminescence intensity of the first experiment is 38.6% larger than the second experiment, the mean heat release rate is 39% less. The instantaneous chemiluminescence intensity is an integral of the specific chemiluminescence yield per unit air consumption rate along the flame front, and the instantaneous heat release rate is proportional to the integral of the instantaneous air consumption rate along the flame front. Both the instantaneous chemiluminescence and the instantaneous heat release rate are directly affected by the time-varying flame surface area. With fuel modulations off the acoustic resonant frequencies, variations in the airflow rate across the air swirler are usually negligibly small. Thus. flame surface area variations are mainly caused by equivalence ratio perturbations along the flame front. The location of a laminar flamelet is determined by the dynamics of the upstream reactant velocity and the laminar burning velocity. The laminar burning velocity is a highly nonlinear function of the equivalence ratio. Equivalence ratio perturbations along the flame front are always accompanied by variations in the laminar burning velocity and, consequently, in the flame surface area. Although both the chemiluminescence yield and the heat release rate are proportional to the flame surface area, the sensitivity of the laminar flame speed and the chemiluminescence yield to the equivalence ratio is different. This may explain the phase differences between the instantaneous chemiluminescence intensity and the instantaneous heat release rate during unsteady combustion.

Figure 11 shows the time traces of several parameters with fuel modulations at 297 and 874 Hz, respectively. These parameters are CH* chemiluminescence, the estimated instantaneous air consumption rate, the estimated instantaneous equivalence ratio, the estimated instantaneous heat release rate, and the fuel pressure 0.29 m upstream of the fuel nozzle. All parameters are normalized by their mean quantity. All data are filtered using a fourth-order Butterworth filter with a bandwidth of 200 Hz around the fuel modulation frequency. The amplitude of the normalized CH* chemiluminescence is five times larger than that of the heat release rate. In both cases, substantial phase differences exist between CH* chemiluminescence and the other parameters. With fuel modulations at 297 and 874 Hz, the instantaneous heat release rate lags chemiluminescence in phases by more than 80 deg. However, the phase differences among the equivalence ratio, the air consumption rate, and the heat release rate are rather small. From Fig. 11, one can see that variations in the normalized air consumption rate are comparable to those in the normalized equivalence ratio. This implies that fuel modulations have resulted in large variations in the flame suface area. For lean fuel/air mixtures, the laminar flame speed is exponentially sensitive to the equivalence ratio. A linear analysis of an inverted laminar

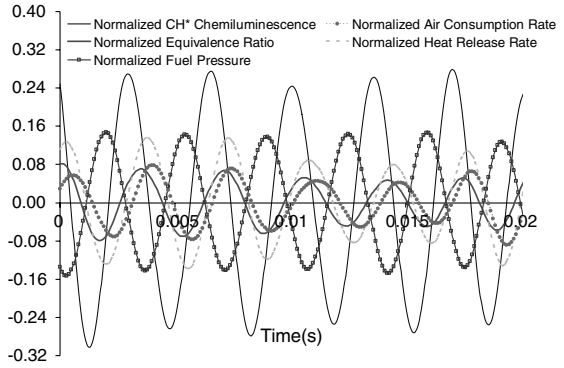

a)

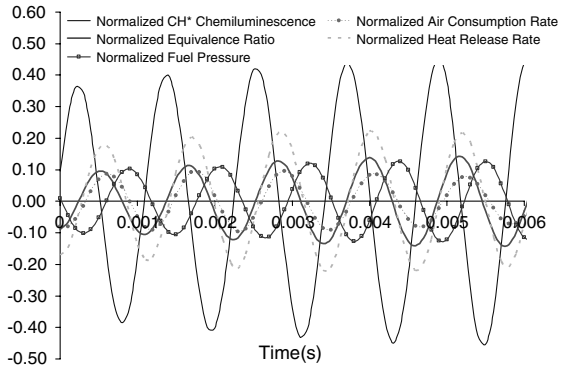

b)

Fig. 11 Time traces of CH* chemiluminescence, the estimated air consumption rate, the estimated representative equivalence ratio, the estimated heat release rate, and the fuel pressure: a) fuel modulations at 296 Hz, and b) fuel modulations at 874 Hz. All parameters are normalized by their mean quantity.

V flame shows that, for unsteady combustion involving equivalence ratio perturbations, the dynamics of the flame surface area can be modeled as a first-order system with a negative high-frequency gain. That is, the phase lag between the flame surface area and the equivalence ratio approaches 270 deg with increasing frequency. Figures 11a and 11b show that chemiluminescence lags the equivalence ratio in phases by about 270 deg. This implies that, although the chemiluminescence yield per unit air consumption rate does increase with the equivalence ratio, the overall chemiluminescence intensity decreases because of larger reductions in the instantaneous flame surface area.

VI. Discussion

The correlation functions are derived for the present liquid-fueled, swirl-stabilized, LDI combustor and are accurate for the described working range. For different combustors, the same procedures can be applied to develop new correlation functions. The reported strategies work best for lean premixed combustion, for which the fuel/air equivalence ratio is uniform upstream of the flame front. For the present liquid-fueled combustor, because of the small droplet size and fast fuel/air mixing, the fuel/air equivalence ratio upstream of the flame front is roughly uniform. This allows a globally representative equivalence ratio to be used.

For unsteady combustion, the estimated instantaneous air consumption rate and equivalence ratios along the flame front should not be considered the same as those at the combustor inlet. Because of the complicated physicochemical processes between these two locations, substantial differences in both amplitude and phases exist.

Quasi-steady relationships among the heat release rate, the air consumption rate, the equivalence ratio, and the preheat temperature are assumed for unsteady combustion. This is valid for the present combustor. The quasi-steady relationship is also applicable to combustion instability involving acoustically synchronized large vortex shedding. This is because, in such cases, the flame curvature radius is typically much larger than the flame thickness.

Pressure effects on chemiluminescence yield are taken into account in the determination of the instantaneous heat release rate and equivalence ratios. Quasi-steady responses among the combustor pressure, chemical kinetics, and chemiluminscence production are assumed. This assumption has been widely used in the combustion community and is valid at least at low frequencies. The lifetime of radical species or the time scale of photo release is at least 3 orders of magnitude smaller than the acoustic cycle [17]; thus, the chemiluminescence yield can be assumed instantaneous with the chemical reaction rate.

VII. Conclusions

1) Flame spectra of the present turbulent, liquid-fueled, swirl-stabilized, LDI combustor are very similar to those of lean premixed gaseous combustion. This can be attributed to the small droplet size and fast fuel/air mixing. Background emissions around 431 nm, which mainly consist of CO_2^* chemiluminescence, are found to be self-similar with wavelength within a broad range of working conditions. This implies that background emissions around 431 nm can be determined from emission measurements near 431 nm.

2) Accurate correlation functions, which express chemiluminescence as a function of the airflow rate, the equivalence ratio, and the preheat temperature, are developed for combustion within a large range of working conditions. The average error between measurements and correlation in the mean chemiluminescence is within 2.37% for OH^*, 1.96% for CO_2^*, and 3.8% for CH^*.

3) Procedures for the determination of the instantaneous air consumption rate and the instantaneous equivalence ratio along the flame front are developed. For both self-excited combustion instability and forced flame responses under fuel modulations, the errors in the estimated mean heat release rate, the estimated mean air consumption rate, and the estimated mean equivalence ratio are below 2.0%.

4) The assumption that chemiluminescence is proportional to the instantaneous heat release rate is generally invalid. During self-excited combustion instability, both the gain and phases between heat release and chemiluminescence vary with the acoustic oscillation intensity. During forced flame responses, the gain varies with frequency by more than 20% and the phase lag consistently increases with frequency up to 96 deg above 400 Hz. This can be attributed to the differences in the sensitivity to equivalence ratios among the chemiluminescence yield, the heat release rate, and the flame surface area.

5) Acoustic oscillations are isentropic, but both acoustic pressure and acoustic temperature affect the chemiluminescence yield. Acoustics-induced chemiluminescence oscillations are taken into account for the determination of the instantaneous heat release rate and the instantaneous equivalence ratio.

6) The developed strategies can be applied to other combustion systems and work best for lean premixed combustion with a compact flame.

Acknowledgments

Support from NASA John H. Glenn Research Center at Lewis Field under grant NNX07C98A, “Active Combustion Control for Low-Emission Combustors,” is gratefully acknowledged. Clarence Chang is the project manager. This project is also supported by the U.S. Air Force under grant FA9550-07-1-0451, “Advanced Thermally Stable Coal-Based Jet Fuels.” The authors would like to thank P. Stephen and B. Quay for sharing the PMT housing and Robert Santoro for sharing the spectrometer.

References

[1] Najm, H. N., Paul, P. H., Mueller, C. J., and Wyckoff, P. S., “On the Adequacy of Certain Experimental Observables as Measurements of Flame Burning Rate,” *Combustion and Flame*, Vol. 113, No. 3, 1998, pp. 312–332.

doi:10.1016/S0010-2180(97)00209-5
[2] Paul, P. H., and Najm, H. N., "Planar Laser-Induced Fluorescence Imaging of Flame Heat Release Rate," *Proceedings of the Combustion Institute*, Vol. 27, 1998, pp. 43–50.doi:10.1016/S0082-0784(98)80388-3
[3] Ayoola, B. O., Balachandran, R., Frank, J. H., Mastorakos, E., and Kaminski, C. F., "Spatially Resolved Heat Release Rate Measurements in Turbulent Premixed Flames," *Combustion and Flame*, Vol. 144, 2006, pp. 1–16.
doi:10.1016/j.combustflame.2005.06.005
[4] Baranger, P., Orain, M., and Grisch, F., "Fluorescence Spectroscopy of Kerosene Vapour: Application to Gas Turbines," AIAA Paper 2005-828, Jan. 2005.
[5] Klingbeil, E., Jeffries, J. B., and Hanson, R. K., "Temperature- and Pressure-Dependent Absorption Cross Sections of Gaseous Hydrocarbons at 3.39 μm," *Measurement Science and Technology*, Vol. 17, 2006, pp. 1950–1957.
doi:10.1088/0957-0233/17/7/038
[6] Drallmeier, J. A., "Hydrocarbon-Vapor Measurements in Pulsed Fuel Sprays," *Applied Optics*, Vol. 33, No. 33, 1994, pp. 7781–7788.
doi:10.1364/AO.33.007781
[7] Kojima, J., Ikeda, Y., and Nakajima, T., "Basic Aspects of OH(A), CH (A), and C2(d) Chemiluminescence in the Reaction Zone of Laminar Methane–Air Premixed Flames," *Combustion and Flame*, Vol. 140, 2005, pp. 34–45.
doi:10.1016/j.combustflame.2004.10.002
[8] Muruganandam, T. M., Kim, B. H., Morrell, M. R., Nori, V., Patel, M., Romig, B. W., and Seitzman, J. M., "Optical Equivalence Ratio Sensors for Gas Turbine Combustors," *Proceedings of the Combustion Institute*, Vol. 30, 2005, pp. 1601–1609.
doi:10.1016/j.proci.2004.08.247
[9] Chou, T., and Patterson, D. J., "In-Cylinder Measurement of Mixture Maldistribution in a L-Head Engine," *Combustion and Flame*, Vol. 101, 1995, pp. 45–57.
doi:10.1016/0010-2180(94)00174-Q
[10] Hardalupas, Y., and Orain, M., "Local Measurements of the Time-Dependent Heat Release Rate and Equivalence Ratio Using Chemiluminescent Emission from a Flame," *Combustion and Flame*, Vol. 139, 2004, pp. 188–207.
doi:10.1016/j.combustflame.2004.08.003
[11] Markstein, G. H., *Nonsteady Flame Propagation*, MacMillan, New York/Indianapolis, IN, 1964, pp. 5–13.
[12] Samaniego, J. M., Egolfopoulos, F. N., and Bowman, C. T., "CO_2^* Chemiluminescence in Premixed Flames," *Combustion Science and Technology*, Vol. 109, 1995, pp. 183–203.
doi:10.1080/00102209508951901
[13] Egolfopoulos, F. N., and Campbell, C. S., "Unsteady Counterflowing Strained Diffusion Flames: Diffusion-Limited Frequency Response," *Journal of Fluid Mechanics*, Vol. 318, 1996, pp. 1–29.
doi:10.1017/S0022112096007008
[14] Lee, J. G., Gonzalez, E., and Santavicca, D. A., "On the Application of Chemiluminescence to the Estimation of Unsteady Heat Release During Unstable Combustion in Lean Premixed Combustor," AIAA Paper 2005-3575, 2005.
[15] Higgins, B., McQuay, M. Q., Lacas, F., Rolon, J. C., Darabiha, N., and Candel, S., "Systematic Measurements of OH Chemiluminescence for Fuel-Lean, High-Pressure, Premixed, Laminar Flames," *Fuel*, Vol. 80, 2001, pp. 67–74.
doi:10.1016/S0016-2361(00)00069-7
[16] Higgins, B., McQuay, M. Q., Lacas, F., and Candel, S., "An Experimental Study on the Effect of Pressure and Strain Rate on CH Chemiluminescence in Premixed Fuel-Lean Methane/Air Flame," *Fuel*, Vol. 80, 2001, pp. 1583–1591.
doi:10.1016/S0016-2361(01)00040-0
[17] Gordan, A. G., *Spectroscopy of Flames*, Chapman and Hall, London, 1974, pp. 13, 164, and 166.
[18] Turns, S. R., *An Introduction to Combustion: Concepts and Applications*, 2nd ed., McGraw–Hill, New York, 2000, pp. 362–378, 461.
[19] Yi, T., and Santavicca, D. A., "Combustion Instability in a Turbulent Liquid-Fueled Swirl-Stabilized LDI Combustor: I. Experiments," AIAA Paper 2009-5014, Aug. 2009.
[20] Culick, F. E. C., "Combustion Instabilities in Liquid-Fueled Propulsion Systems—An Overview," CP-450, AGARD/NATO, Neuilly-sur-Seine, France, 1989.
[21] Syred, N., and Beer, J. M., "Combustion in Swirling Flows: a Review," *Combustion and Flame*, Vol. 23, No. 2, 1974, pp. 143–201.
doi:10.1016/0010-2180(74)90057-1
[22] Lilly, D. G., "Swirling Flow in Combustion: A Review," *AIAA Journal*, Vol. 15, No. 8, 1977, pp. 1063–1078.
doi:10.2514/3.60756
[23] Anderson, T., and Morford, S., "Dynamic Flame Structure in a Low NO_x Premixed Combustor," American Society of Mechanical Engineers Paper GT98-568, June 1998.
[24] Eckstein, J., Freitag, E., Hirsch, C., Sattelmayer, T., Von Der Bank, R., and Schilling, T., "Forced Low-Frequency Spray Characteristics of a Generic Airblast Swirl Diffusion Burner," *Journal of Engineering for Gas Turbines and Power*, Vol. 127, 2005, pp. 301–306.
doi:10.1115/1.1789515
[25] Balachandran, R., Ayoola, B. O., Kaminski, C. F., Dowling, A. P., and Mastorakos, E., "Experimental Investigation of the Nonlinear Response of Turbulent Premixed Flames to Imposed Inlet Velocity Oscillations," *Combustion and Flame*, Vol. 143, 2005, pp. 37–55.
doi:10.1016/j.combustflame.2005.04.009
[26] Yi, T., and Santavicca, D. A., "Flame Transfer Functions and their Applications to Combustion Analysis and Control," American Society of Mechanical Engineers Paper GT2009-60181, June 2009.

A. Gupta
Associate Editor